THE ASTROPHYSICAL JOURNAL, 495:385–400, 1998 March 1

ACCRETION AND THE EVOLUTION OF T TAURI DISKS

LEE HARTMANN,[1] NURIA CALVET,[1,2] ERIK GULLBRING,[1] AND PAOLA D'ALESSIO[3]

Received 1997 June 23; accepted 1997 October 9

ABSTRACT

Using results and calibrations from a previous paper (Gullbring et al. 1997), we estimate disk accretion rates for pre–main-sequence stars in the Taurus and Chamaeleon I molecular cloud complexes. The median accretion rate for T Tauri stars of age ~ 1 Myr is $\sim 10^{-8}$ $M_{\odot}$ yr^{-1}; the intrinsic scatter at a given age may be as large as 1 order of magnitude. There is a clear decline of mass accretion rates $\dot{M}$ with increasing age t among T Tauri stars. Representing this decline as $\dot{M} \propto t^{-\eta}$, we estimate $1.5 \lesssim \eta \lesssim 2.8$; the large uncertainty is due to the wide range of accretion rates at a given age, the limited age range of the sample, and errors in estimating stellar ages and accretion luminosities. Adopting values of η near the low end of this range, which are more likely given probable errors and the neglect of birthline age corrections, masses accreted during the T Tauri phase are roughly consistent with disk masses estimated from millimeter-wave dust emission. Similarity solutions for evolving, expanding disks are used to investigate observational constraints on disk properties employing a minimum of parameters. For an assumed power-law form of the disk viscosity with radius $\nu \propto R^{\gamma}$, $\eta \gtrsim 1.5$ corresponds to $\gamma \gtrsim 1$. The limit $\gamma \sim 1$ corresponds to a roughly constant "α" in the Shakura-Sunyaev (1973) viscosity parameterization; using current observed disk sizes, we estimate $\alpha \sim 10^{-2}$ (on scales $\sim$10–100 AU). Much of the observed variation in mass accretion rates can be accounted for by varying initial disk masses between 0.01 and 0.2 $M_{\odot}$, but this result may be strongly affected by the presence of binary companion stars. These results emphasize the need for older samples of stars for studying disk evolution.

Subject headings: accretion, accretion disks — circumstellar matter — stars: formation — stars: pre–main-sequence

1. INTRODUCTION

It has long been apparent from the evidence of the solar system that disks could play an important role in the formation of stars and planets. The idea that the solar nebula was an accretion disk has been developed extensively since the early papers of von Weisäcker (1948) and Lüst (1952) (see discussion in Pringle 1981). The seminal paper of Lynden-Bell & Pringle (1974), which explained the activity of T Tauri stars in terms of disk accretion, foreshadowed the present view that disks are commonly found in early stellar evolution (Strom et al. 1989; Skrutskie et al. 1990; Beckwith et al. 1990, hereafter BSCG).

Currently there is a large and growing body of observational estimates of T Tauri disk masses and sizes (BSCG; Osterloh & Beckwith 1995, hereafter OB; Dutrey et al. 1995; Keene & Masson 1990; Lay et al. 1994; Dutrey et al. 1995; McCaughrean & O'Dell 1996). Much less progress has been made in understanding the evolution of T Tauri disks, largely because of the small age range in present samples of accreting stars. The issue is complicated by the possibility of grain evolution. Most detections of disks rely upon observations of dust emission; disk masses are thus dependent upon assumed dust opacities, which may be different from those in the interstellar medium (e.g., Beckwith & Sargent 1991).

The rate of mass accretion $\dot{M}$ through T Tauri disks is an important parameter for several reasons. Local disk structure is affected by rate of mass flow, which in turn is determined by the rate of gravitational energy release. Disk evolution also depends upon the accretion rate. In a simple viscous disk, the rate at which material is removed is given by the accretion rate onto the central star; at the same time, the disk must expand to account for the angular momentum lost by the accreting material. The rate at which this accretion and angular momentum transfer occurs is proportional to the viscosity, so the evolution of the disk can be predicted if the viscosity is known. An initial attempt to calculate the evolution of the solar nebula accounting for disk expansion was made by Ruden & Pollack (1991); however, their assumption of a convective viscosity led to large disk masses left over at the end of accretion, which may be incorrect if convection is not the source of disk angular momentum transport (Ryu & Goodman 1992; Stone & Balbus 1996).

Given the present theoretical difficulties in understanding and predicting disk viscosity, we invert the problem and consider how observations may constrain disk evolution. In this paper we use improved mass accretion rates for T Tauri stars presented in a companion paper (Gullbring et al. 1997, hereafter Paper I) to constrain the physical conditions in, and evolution of, T Tauri disks. We employ similarity solutions for viscous disks that enable us to interpret the observed relationships between the disk masses, accretion rates, sizes, and ages using a minimum number of parameters and theoretical preconceptions. The models also make predictions for disk structure and evolution that can be tested by future observations. The similarity solutions presented here can serve as the starting point for more complex models that will be developed and tested as observational techniques improve.

2. MASS ACCRETION RATES VERSUS AGE

In Paper I we determined mass accretion rates from medium-resolution spectrophotometric measurements of

[1] Harvard-Smithsonian Center for Astrophysics, 60 Garden Street, Cambridge, MA 02138; ncalvet@cfa.harvard.edu, lhartmann@cfa.harvard.edu, egullbring@cfa.harvard.edu.

[2] Also Centro de Investigaciones de Astronomia, A.P. 264, Mérida, Venezuela.

[3] Instituto de Astronomía, Universidad Nacional Autónoma de México, A.P. 70-264, 04510 México D.F., México; dalessio@astroscu.unam.mx.

the hot continuum emission of 17 pre–main-sequence stars in the Taurus-Auriga molecular complex. We also developed a method by which accretion rates can be estimated from broadband photometry and optical spectral types. Here we employ these methods to develop a statistical picture of mass accretion rates of T Tauri stars as a function of age.

We supplemented our medium-resolution spectrophotometric results from Paper I with estimates derived from broadband photometry, as also described in Paper I. Briefly, in the photometric method the accretion luminosity is determined from the excess emission in the U bandpass, corrected for extinction using the $V-R$ colors of the star and its spectral type. The photometry and spectral types were taken from Kenyon & Hartmann (1995, hereafter KH). The final conversion from U excess emission to bolometric accretion luminosity is derived by comparison with stars analyzed in detail using spectrophotometry. The stellar luminosities are derived from the reddening corrected J magnitude as described in KH (this procedure minimizes extinction corrections). We eliminated stars with very large accretion luminosities, for which our methods (and most others) fail. Using the spectral type and effective temperatures given in KH, we can derive the stellar radius and place the star in the H-R diagram. Finally, we determine the stellar mass and age from the H-R diagram position using the Canuto-Mazzitelli-Alexander ("CMA") evolutionary tracks of D'Antona & Mazzitelli (1994). The mass accretion rate is then derived from the relation

$$L_{\rm acc} = 0.8\,\frac{GM_*\dot{M}}{R_*}\,, \qquad (1)$$

where M_* and R_* are the stellar mass and radius, respectively, and the factor in front on the right-hand side comes from assuming that the hot continuum luminosity represents the dissipation of accretion energy as material falls in freely along the stellar magnetosphere from a radius $\sim 5R_*$ (which is close to the typical corotation radius; Shu et al. 1994).

2.1. *Correlation of Accretion Rates with Ages in Taurus*

In Table 1 we list mass accretion rates and stellar properties for Taurus pre–main-sequence stars in the spectral type

TABLE 1

ACCRETION RATES FOR TAURUS PMS STARS

Object (1)	Spectral Type (2)	log $L_*/L_\odot$ (3)	log $L_{\rm acc}/L_\odot$ (4)	$M_*/M_\odot$ (5)	$R_*/R_\odot$ (6)	log $\dot{M}$ (7)	log t (8)	Source (9)
AA Tau	K7	−0.15	−1.60	0.53	1.74	−8.48	5.98	b
BP Tau	K7	−0.03	−0.75	0.49	1.99	−7.54	5.79	b
CY Tau	M1	−0.31	−1.34	0.42	1.63	−8.12	6.32	b
DE Tau	M2	−0.06	−1.15	0.25	2.45	−7.58	5.02	b
DF Tau	M0.5	0.13	−0.45	0.27	3.37	−6.91	5.09	b
DK Tau	K7	0.16	−0.78	0.43	2.49	−7.42	5.56	b
DN Tau	M0	−0.06	−1.80	0.38	2.09	−8.46	5.69	b
DO Tau	M0	0.00	−0.22	0.37	2.25	−6.84	5.63	b
DQ Tau	M0	−0.20	−2.40	0.44	1.79	−9.40	5.88	b
DS Tau	K5	−0.24	−0.68	0.87	1.36	−7.89	6.58	b
GG Tau	K7	0.10	−1.08	0.44	2.31	−7.76	5.63	b
GI Tau	K6	−0.07	−1.03	0.71	1.48	−8.02	6.09	b
GK Tau	K7	0.03	−1.46	0.46	2.15	−8.19	5.70	b
GM Aur	K7	−0.13	−1.15	0.52	1.78	−8.02	5.95	b
HN Tau	K5	−0.72	−1.46	0.81	0.76	−8.89	7.48	b
IP Tau	M0	−0.39	−2.15	0.52	1.44	−9.10	6.23	b
UY Aur	K7	0.02	−0.57	0.42	2.60	−7.18	5.52	b
CI Tau	K7	−0.09	−0.36	0.50	1.87	−7.19	5.87	U
CX Tau	M2.5	−0.43	−2.26	0.33	1.63	−8.97	5.93	U
CZ Tau	M1.5	−0.67	−2.40	0.41	1.19	−9.35	6.40	U
DM Tau	M1	−0.50	−1.05	0.43	1.39	−7.95	6.19	U
DD Tau	M1	−0.47	−1.52	0.42	1.44	−8.39	6.14	U
DH Tau	M1	−0.34	−1.54	0.38	1.67	−8.30	5.92	U
DI Tau	M0	−0.25	−1.95	0.43	1.71	−8.75	5.92	U
DP Tau	M0.5	−0.44	−0.98	0.46	1.44	−7.88	6.17	U
FM Tau	M0	−0.59	−1.36	0.58	1.17	−8.45	6.61	U
FO Tau	M2	−0.44	−0.78	0.33	1.59	−7.50	5.95	U
FQ Tau	M2	−0.54	0.34	0.35	1.42	−6.45	6.09	U
FS Tau	M1	−0.59	−1.13	0.46	1.25	−8.09	6.38	U
FV Tau	K5	0.03	0.75	0.71	1.87	−6.23	6.02	U
FX Tau	M1	−0.21	−2.00	0.34	1.94	−8.65	5.76	U
FY Tau	K7	−0.08	−0.58	0.50	1.87	−7.41	5.87	U
GH Tau	M2	−0.29	−1.32	0.29	1.90	−7.92	5.77	U
GO Tau	M0	−0.43	−0.98	0.50	1.40	−7.93	6.25	U
Haro 6−37	K6	−0.01	−0.10	0.60	1.90	−7.00	5.92	U
HO Tau	M0.5	−0.81	−1.68	0.56	0.94	−8.86	6.92	U
IQ Tau	M0.5	−0.14	−0.90	0.35	2.01	−7.55	5.73	U
LkCa 15	K5	−0.14	−1.75	0.81	1.53	−8.87	6.37	U
LkHa 332/G1	M1	−0.04	−0.10	0.29	2.36	−6.60	5.31	U
V955 Tau	K7	0.11	−0.349	0.44	2.34	−7.02	5.61	U

NOTES.—Mass accretion rates (col. [6]) are in $M_\odot$ yr^{-1}. Source (col. [9]) indicates method of determining accretion luminosities and mass accretion rates: b, blue spectrum analysis from Paper I; U, photometric calibration from Paper I, using mean U magnitude from KH.

range K5–M2. We chose this range for several reasons. First, many T Tauri stars in the region lie within these spectral type limits, and our detailed spectrophotometric results are mostly for such stars. Second, we wished to minimize problems in correcting for reddening, which become greater for cooler stars, and to avoid introducing biases against observing faint ultraviolet accretion emission that would occur in hotter, more luminous stars. Third, by restricting our effective temperature range we hope to minimize problems due to uncertainties in stellar evolutionary tracks; adoption of different theoretical calculations would change the absolute ages of the stars, but would have less effect on the *relative* stellar ages.

Figure 1*a* shows the accretion rates for the Taurus stars vs. age, with the values derived from detailed spectrophotometry as solid circles and the estimates from the broadband photometry as open circles. The two different methods—spectrophotometry and broadband measurements—produce consistent results. There is a clear trend of decreasing mass accretion rates with increasing stellar age, qualitatively as initially identified by Hartigan, Edwards, & Ghandour (1995). The correlation coefficient for the whole sample is approximately $r \sim -0.5$, and the nonparametric Spearman rank-order correlation (e.g., Press et al. 1986) indicates that the probability that the data are randomly distributed is less than 10^{-3}.

We do not think that correlated errors can be responsible for the trend shown in Figure 1*a*, because there is no effect that we can identify which would produce important errors of similar magnitude in L_* and $L_{\rm acc}$. For example, an error in distance would affect L_* and $L_{\rm acc}$ in the same way and thus produce a correlated error. However, it is implausible that *variations* in the distances to individual Taurus stars can account for the observed range of measurements. One might guess that the depth of the cloud complex in the line of sight is similar to its lateral extent; this would suggest distance variations of about 20 pc out of an average distance of 140 pc (Kenyon & Hartmann 1995); this would account for a scatter of only about 0.25 dex in the age or in $\dot{M}$), which is small compared with the ranges shown in Figure 1*a*. Moreover, although the slope of the trend of $\dot{M}$ vs. t is uncertain, it appears to be steeper than that which one would expect from distance errors, as discussed in the following subsection (§ 2.2); in other words, the accretion luminosity appears to decrease faster with increasing age than does the stellar luminosity.

Other possible sources of error seem even less plausible as the cause of the observed correlation. For example, an error in extinction would affect both accretion and stellar luminosities in the same direction; but by using near-infrared fluxes to estimate the stellar luminosity, we minimize the extinction corrections. For typical values $A_V \sim 1$, the extinction at the J band—and thus the correction needed to obtain the stellar luminosity—is only ~ 0.36 mag (Mathis 1990), resulting in only a very modest correction to the stellar age. In contrast, the typical extinction at U is ~ 2 mag, so that the hot continuum accretion luminosity is much more sensitive to the extinction. Unresolved binary companion stars can make the apparent luminosity of the "single star" erroneously large; however, this will not directly affect the accretion luminosity estimates, which depend mostly on the excess Balmer continuum emission (Paper I). We conclude that the trend observed in Figure 1*a* is intrinsic and shows that mass accretion rates decrease with increasing age for the Taurus K5–M2 sample.

2.2. *Constraints on $\dot{M}(t)$*

Having demonstrated the existence of a significant correlation between $\dot{M}$ and t, we next turn to the more difficult problem of quantifying this relation. To do so we need to consider several possible sources of error, both systematic and random, in addition to the dispersion due to intrinsic differences in the accretion rates of stars of the same age.

Systematic errors in determining the accretion rates arise from uncertainties in extinction and from the significant bolometric corrections needed to account for the unobserved portion of the accretion luminosity (Paper I). Although we suggested in Paper I that the magnitude of systematic error might be as much as a factor of 3, this estimate is uncertain, and further ultraviolet observations are needed to explore this further. Similarly, there may also be systematic errors in age determinations. Because there are currently no direct mass measurements for T Tauri stars, ages depend upon comparing observed H-R diagram positions with theoretical evolutionary tracks, which may differ due to differing treatments of convection, atmospheric

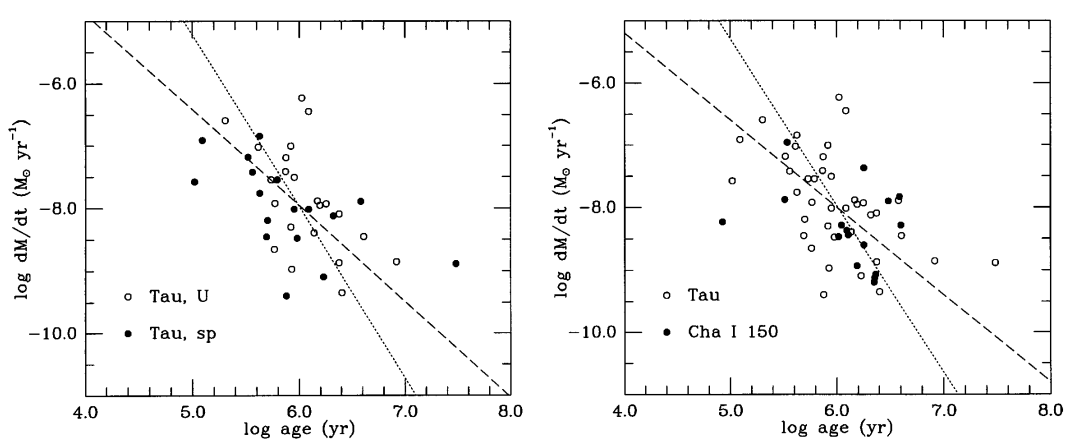

FIG. 1.—Mass accretion rate vs. age. (*a*) Stars in the Taurus sample; indicated are stars with mass accretion rate from blue spectrophotometry (*filled circles*) and from U magnitudes (*open circles*); (*b*) Stars in Taurus (*open circles*) and in Chamaeleon I (*filled circles*), the last at a distance of 150 pc. *Dashed lines*, least-square best-fit assuming that the error in log t is 0.3, while the error in log dM/dt is 0.6. *Dotted lines*, least-square best-fit assuming that the error in both log t and log dM/dt are 0.4. The dashed line fits are preferred because the errors in estimating accretion rates, along with the intrinsic dispersion of accretion at a given age, are likely to be larger than the differential errors in stellar ages (see text).

opacities, etc., resulting in systematic changes in ages by as much as a factor of 2 in the relevant mass range (cf. Mazzitelli 1989).

The slope η of the log $\dot{M}$—log t relation is sensitive to differential errors. By restricting our analysis to a limited range in spectral type or effective temperature, which limits the sample to stars of similar mass, we have attempted to minimize differential errors in ages; however, "birthline" age corrections could have a significant effect on η. The ages in Figure 1 are derived from the Hayashi track evolution calculations of D'Antona & Mazzitelli (1994), which start contraction from (effectively) infinite radius. In reality, at the end of protostellar infall, low-mass stars probably have finite radii and lie along a "birthline" (Stahler 1983, 1988); this would imply that the Hayashi track ages of the youngest stars in Figure 1 can be overestimated substantially. Current models suggest that the low-mass birthline corresponds roughly to the 3×10^5 yr isochrone in the D'Antona & Mazzitelli (1994) CMA tracks (see Hartmann, Cassen, & Kenyon 1997 for a discussion); this suggests that the youngest stars in Figure 1 should be shifted preferentially to the left, which would tend to flatten the $\dot{M}$ vs. t relation (smaller values of η). However, there is substantial uncertainty in birthline ages, and so we simply note this problem without attempting to make a correction.

It is evident from Figure 1, as well as from the value of the correlation coefficient, that there is substantial scatter in the accretion rate-age relation. Some of this dispersion may well be due to intrinsic variations in $\dot{M}$ among stars of a given age, as well as time-variability of individual stars. Differential errors in the accretion rates are much harder to estimate; in Paper I we suggested that the uncertainties in $\dot{M}$ due to geometry, variability, etc. may be about a factor of 3 for an individual star. A previous analysis (Kenyon & Hartmann 1995) suggested that random errors in determining stellar luminosities for K7–M2 stars in Taurus might lead to errors in ages of a factor of 3. This estimate now seems somewhat high, as that study assumed that disks reach to the stellar surface and are not truncated by a magnetosphere; the effect is to increase the occultation of the stellar photosphere by the disk relative to that produced by disks with inner holes. In addition, the accretion luminosities assumed by Kenyon & Hartmann (1995), which must be taken into account in any determination the stellar luminosity, are substantially higher than estimated here. A reasonable guess at for the random errors in the ages of our Taurus stars (apart from systematic errors due to evolutionary track calibrations) is probably a factor of 2 (corresponding to an uncertainty of about 50% in the stellar luminosity; cf. eq. [2]).

Based on these considerations, we initially examined fits to the data of Figure 1*a* using minimum errors of factors of ~ 2 in the ages and $\gtrsim 3$ in the accretion rates. Least-square best-fit straight lines were determined for the Taurus data in the form of log $\dot{M}$ vs. log t. We found that the results for the slope η in the relation $\log \dot{M} \propto -\eta \log t$ depends critically on the assumed relative sizes of the errors in t and $\dot{M}$. If $\sigma(\log t) < \sigma(\log \dot{M})$, then we found $\eta \sim 1.5 \pm 0.3$. Conversely, if $\sigma(\log t) > \sigma(\log \dot{M})$, then we found $\eta \sim 2.7 \pm 0.7$. The results for the Taurus sample are also sensitive to whether we include the oldest star in this sample, HN Tau, or not. If we eliminate this star, even assuming that the age error is less than the error in accretion rates, we find $\eta \sim 2.1 \pm 0.5$.

The difficulty in estimating η is the limited age range of the Taurus sample, coupled with the large spread in measured accretion rates at a given age. We therefore supplemented the Taurus results with data for pre–main-sequence stars of the Chamaeleon I association in the K5–M2 spectral type region. We were motivated to include the Cha I sample because it has been suggested that its pre–main-sequence stellar population is older and thus may provide a wider age range to improve constraints on the decay rate of mass accretion. The data were taken from the compilation by Gauvin & Strom (1992), and the accretion rates and stellar ages were derived from the photometry and spectral types as for the Taurus sample. Unfortunately, there is controversy about the correct distance to Cha I, with estimates ranging from about 140 to 200 pc, as summarized by Schwartz (1991). While Schwartz suggests that a consensus seems to be developing for a distance of $\sim 150 \pm 15$ pc (see also Steenman & Thé 1989), the situation remains somewhat uncertain.

Figure 1*b* shows the results of adding the Cha I sample to the Taurus sample adopting a distance of 150 pc (see also Table 2). The addition of these few stars do not change the results from those of Taurus in any substantial way, although now the fits do not depend strongly on the inclusion or exclusion of any single star. Adopting our best estimates for errors of 0.3 in log t and 0.6 in log $\dot{M}$, we find $\log (\dot{M}/M_\odot \text{ yr}^{-1}) = -8.00 \pm 0.10 - (1.40 \pm 0.29) \log (t/10^6 \text{ yr})$. This is our preferred result, not correcting for birthline age effects. However, it must be noted that it is difficult to rule out a steeper decay in the mass accretion rate with time, given the uncertainty in errors; for errors of 0.4 in both log t and in log $\dot{M}$, we find $\log (\dot{M}/M_\odot \text{ yr}^{-1}) = -7.97 \pm 0.16 - (2.68 \pm 0.62) \log (t/10^6 \text{ yr})$.

We also considered how our results would differ if we had adopted the two extreme distances of 140 and 200 pc for Cha I. As described in the previous subsection, a change in distance affects both the accretion luminosity and stellar luminosity in a similar way, which tends to produce a correlated shift between accretion rate and age. To make a simple quantitative estimate of the effect, we approximate Hayashi track evolution of the low-mass stars under consideration here as gravitational contraction of a star with a fixed polytropic index (i.e., a completely convective star) and a constant effective temperature. With these assumptions the Hayashi track age (i.e., the contraction age from infinite starting radius) varies with stellar luminosity as (e.g., Stahler 1988)

$$t \propto L_*^{-3/2} . \tag{2}$$

Changing the distance affects the accretion and stellar luminosities equally, so

$$L_{\rm acc} \propto L_* \sim t^{-2/3} . \tag{3}$$

Since the derived mass accretion rate depends on the stellar mass and luminosity in addition to the accretion luminosity, for fixed stellar mass $\dot{M} \propto R_* L_{\rm acc}$. Since $L_* \propto R_*^2$, changing the distance results in a correlated shift of mass accretion rates and ages,

$$\dot{M} \text{ (apparent)} \sim t^{-1} . \tag{4}$$

Our detailed results using the CMA tracks of D'Antona & Mazzitelli (1994) agree with this estimate fairly well. Since this shift is not very different than the main trend of the Taurus data points, and since there are fewer Cha I stars

TABLE 2

ACCRETION RATES FOR CHA I PMS STARS

Object	Spectral Type	log $L_*/L_\odot$	log $L_{acc}/L_\odot$	$M_*/M_\odot$	$R_*/R_\odot$	log $\dot{M}$	log t	Source
CT Cha	K7	−0.18	−1.36	0.55	1.67	−8.28	6.05	U
HM 8	M0.5	−0.58	−0.74	0.57	1.18	−7.83	6.59	U
HM 12	M2	−0.71	−2.30	0.36	1.17	−9.20	6.35	U
HM 15	M0.5	−0.40	−2.00	0.49	1.44	−8.94	6.19	U
HM 32	M0.5	−0.48	−2.12	0.53	1.33	−9.12	6.36	U
SX Cha.....	M0.5	−0.35	−1.48	0.47	1.53	−8.37	6.09	U
SY Cha.....	M0	−0.43	−1.64	0.50	1.40	−8.60	6.26	U
UY Cha	M1.5	0.05	−1.80	0.28	2.62	−8.23	4.93	U
VV Cha	M1	−0.53	−0.45	0.44	1.34	−7.37	6.26	U
VW Cha	K5	0.37	−0.21	0.60	2.75	−6.95	5.54	U
VZ Cha	K6	−0.34	−1.10	0.78	1.30	−8.28	6.60	U
WW Cha.....	K5	0.39	−1.14	0.60	2.82	−7.87	5.51	U
WX Cha	M0	−0.17	−1.56	0.54	1.70	−8.47	6.02	U
WY Cha	K7	−0.21	−1.49	0.57	1.61	−8.44	6.11	U
WZ Cha	M1	−0.64	−0.89	0.47	1.17	−7.90	6.48	U
XX Cha	M1	−0.58	−2.11	0.45	1.26	−9.07	6.36	U

NOTE.—Columns represent same quantities as in Table 1. Photometry taken from Gauvin & Strom 1992.

than Taurus stars, the straight line fits do not significantly change whether 140 or 200 pc is adopted and do not differ much from the results for Taurus alone, although the fits for 200 pc indicate larger uncertainties in the value of η.

We conclude that the relation of $\dot{M}(t)$ vs. t is poorly constrained at present. The slope of the relation lies in the range $\eta \sim 1.5$–2.8, with smaller values being more likely considering the probable errors of measurement and potential birthline corrections for stellar ages. Older samples of stars will be required to determine this relation more firmly.

3. MASS ACCRETION RATES AND DISK MASSES

The amount of mass accreted by a T Tauri star from its disk after time t,

$$M_{acc} = \int_t^\infty dt\dot{M} \ , \tag{5}$$

is obviously a lower limit to the disk mass that remained at t. While it is impossible to follow the accretion process of an individual T Tauri star, if the mass accretion rate varies as a power law for all times as $\dot{M}(t) = \dot{M}(t_0)(t/t_0)^{-\eta}$, where $\eta > 1$, the total mass which will be accreted at times $t > t_0$ is

$$M_{acc} = \frac{\dot{M}(t_0)t_0}{(\eta - 1)} \ . \tag{6}$$

(In certain models of disk accretion, such as those discussed in the following sections, the mass accretion rate at t_0 and η determine the total mass remaining in the disk, even if at some later time the accretion process is terminated by evaporation, formation of planets, etc. before all the mass is accreted.) If $\eta \sim 1.5$, then

$$M_d \sim M_{acc} \sim 2\dot{M}(t_0)t_0 \ . \tag{7}$$

Currently, the only systematic and extensive estimates of T Tauri disk masses have been made by interpreting the mm and submillimeter dust continuum emission (e.g., BSCG, OB). In these analyses, total disk masses are related to the continuum fluxes F_ν by a relation of the form (see, e.g., BSCG)

$$F_\nu \propto \kappa_\nu T_d M_d \ln(R_d/r_1)(1 + \Delta) \ . \tag{8}$$

Here κ_ν is the dust opacity at frequency ν in units of cross section per gram, T_d is the temperature at the outer edge of the disk R_d, r_1 is the radius at which the disk becomes optically thick at ν, and the factor Δ is the ratio of optically thick to optically thin emission at that frequency. In what follows we will use the phrase "dust emission masses" to mean total (gas + dust) disk masses determined from long-wavelength dust emission using a form of equation (8).

While there are uncertainties in estimating disk dust temperatures, and optical depth effects can be important, the dust opacity κ_ν probably represents the most important *systematic* uncertainty in determining disk masses from mm and submillimeter fluxes (BSCG). It has been suggested that the dust opacity is uncertain in the mm range by a factor of 4–5 (Pollack et al. 1994), but even this represents a significant systematic effect. Moreover, there may be evidence for evolution in grain properties from the dust continuum spectra (Beckwith & Sargent 1991), which would suggest even further uncertainty in dust opacities. While the mass estimates from accretion rates are subject to their own substantial uncertainties, particularly in extinctions and bolometric corrections (§ 2.2), these uncertainties are completely independent of the problems involved in estimating disk masses from millimeter-wave emission; moreover, the accretion estimates are independent of any assumed dust opacity, but instead measure the amount of *gas* being accreted.

Before comparing the masses estimated from our accretion rates and equation (7) above with the dust emission masses, it is necessary to make a correction for reasons of consistency. Both BSCG and OB adopt a disk model in which the surface densities and temperatures are power-law distributions; they further adopt a particular form of the opacity, $\kappa_\nu = 0.1(\nu/10^{12}\ \mathrm{Hz})\ \mathrm{g\ cm^{-2}}$. The fluxes also depend on the outer disk radii, with $R_d = 100$ AU usually adopted. Using the disk model of BSCG, and adopting the parameters reported by them, we are able to reproduce the observed 1.3 mm fluxes. However, we are not able to reproduce the observed fluxes in OB using the disk masses and other model parameters listed in their Table 3. We have chosen to multiply the OB disk masses uniformly by a factor of 2.5; with this adjustment, the predicted fluxes agree

TABLE 3

ADOPTED DISK PROPERTIES

Object (1)	F_ν (mJy) (2)	M_d ($M_\odot$) (3)	Multiplicity (4)	Size (2.7 mm) (arcsec) (5)
AA Tau	88	0.021	s	
BP Tau	...	...	s	
CI Tau 190	0.063	s	2 × 0.8	
CX Tau	...	...	u	
CY Tau 133	0.7	s	1 × 0.4	
CZ Tau	...	...	u	
DD Tau	17	0.002	b	
DE Tau	36	0.008	s	
DF Tau	...	...	b	
DH Tau	...	...	u	
DI Tau	...	...	b	
DK Tau	35	0.005	b	
DM Tau	109	0.034	u	
DN Tau	84	0.027	s	1.7 × <1
DO Tau	136	0.018	s	
DP Tau	18	0.003	u	
DQ Tau	91	0.025	b	
DS Tau	24	0.014	s	
FM Tau	...	...	u	
FO Tau	...	...	u	
FQ Tau	...	...	u	
FS Tau	...	...	b	
FV Tau	15	0.001	b	
FX Tau	...	...	s	
FY Tau	16	0.003	u	
GG Tau	593	0.29	b	
GH Tau	...	...	u	
GI Tau	...	...	s	
GK Tau	84	...	s	
GM Aur	253	0.060	s	1.2
GO Tau	83	0.057	u	
Haro 6−37	...	...	u	
HO Tau	...	...	u	
IP Tau	16	0.012	s	
IQ Tau	87	0.040	u	
LkCa 15	167	0.060	u	
LkHa 332/G1	...	...	u	
UY Aur	39	0.003	b	6 × <0.5
V955 Tau	...	...	u	

NOTES.—Fluxes at 1.3 mm (col. [3]) and masses (col. [4]), corrected as described in § 3, taken from BSCG and OB; multiplicity (col. [5]): s, single; b, binary; u, unknown; from Mathieu 1994, Simon & Prato 1995, and Simon et al. 1995; sizes from Dutrey et al. 1995.

quite well with observations if all the other disk parameters remain the same. We therefore ensure that the BSCG and OB data are analyzed in exactly the same way for estimating masses. The adopted disk masses are listed in Table 3, along with estimated sizes from the observations of Dutrey et al. (1995).

Figure 2 compares the results of equation (7) with the dust emission masses from BSCG and OB corrected as described in the previous paragraph. There is an order-of-magnitude scatter of individual data points around a mean value $\log(2\dot{M}t/M_d) = 0.14 \pm 0.23$ (dispersion of the mean). The results suggest that there is no systematic difference between these two different mass estimates, though for any individual object the agreement is less certain. If we eliminate the binary systems (Fig. 2, *open circles*), the result is $\log(2\dot{M}t/M_d) = -0.07 \pm 0.21$ (dispersion of the mean), with a dispersion of a factor of 4 for an individual object.

If we instead had adopted $\eta = 2.8$ in equation (6), the predicted gas masses would be a factor of 3.6 smaller, which would suggest that the dust opacities might be underestimated by a factor of 3. The different results for differing

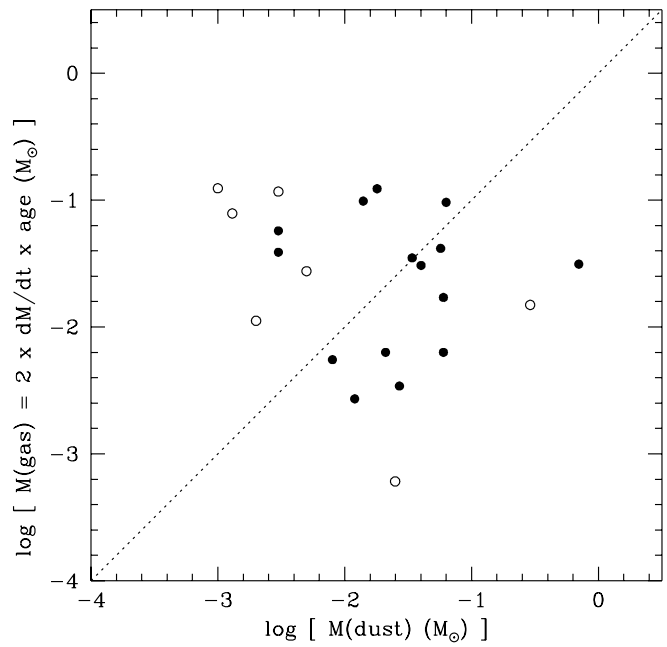

FIG. 2.—Estimated disk mass from accretion rates (*vertical axis*) vs. disk mass estimated from dust emission (*horizontal axis*). The gas mass is determined from the mass accretion rate and the age of each star. The dust emission mass is derived from millimeter flux measurements (Beckwith et al. 1990; Osterloh & Beckwith 1995). The masses from the latter reference have been increased by a factor of 2.5 to match the observed millimeter fluxes (see text). Open circles indicate known binaries (see Table 3).

values of η probably reflect a reasonable estimate of the uncertainty in the results. There are reasons to prefer a smaller value of η. As discussed in § 2.2, birthline age corrections would probably result in a lower slope. Moreover, in § 5.2 we argue that large values of η yield rapid disk expansion rates that are difficult to reconcile with observations. We conclude that the current mass accretion rates and age estimates yield disk masses that show no systematic discrepancy with disk masses estimated from millimeter-wave dust opacities, though samples with larger ranges of ages are needed to make a definitive test.

No correlation is present between the two disk mass estimates in Figure 2. The observed dispersion may not be due only to errors in measuring accretion rates. The dust emission masses depend upon analyzing spectral energy distributions to determine temperatures, the surface density structure is assumed rather than measured, and optical depth effects can be important, even ignoring the possibility of evolution in the dust grain populations (Beckwith & Sargent 1991). The uniqueness of millimeter-wave dust emission mass estimates should be explored further (in the context of fixed dust opacity) to estimate minimum uncertainties.

4. SIMILARITY SOLUTIONS FOR DISK EVOLUTION

The evidence for a decay in disk accretion rates with increasing age suggests that disk evolution is being detected. To explore the significance of the observations further, we examine the properties of simple viscous disk models that may be compared with observations. In these models the only angular momentum transport is provided by viscous stresses, and the accretion of material into the central star must be accompanied by an expansion of the remaining disk material to conserve angular momentum.

Consider a characteristic size scale or radius R_{cd} of a Keplerian disk, defined in terms of its angular momentum J_d and mass M_d,

$$J_d = \int_0^{M_d} dm\Omega R^2 = (GM_*)^{1/2} M_d \langle j \rangle \propto M_d R_{cd}^{1/2} , \quad (9)$$

where Ω is the local angular velocity, dm is an element of mass in the disk, and M_* is the (constant) stellar mass. As long as the inner disk radius is much smaller than R_{cd}, we can set the angular momentum of the accreted material effectively to zero (whether or not the angular momentum is added to the star or is ejected via an inner disk wind; Shu et al. 1994). In this limit, conservation of angular momentum requires $J_d \approx$ constant, and therefore

$$M_d(t) \propto R_{cd}(t)^{-1/2} \quad (10)$$

(see also Cassen 1994). Thus, the rate of decrease of the disk mass with time (and therefore the mass accretion rate) is related to the rate of expansion of the disk, and vice versa. (We restrict the analysis to late phases of disk accretion, when self-gravity of the disk can be neglected, and the central stellar mass does not change appreciably. These assumptions are generally satisfied for the T Tauri stars of our sample, as can be demonstrated a posteriori.)

Given the limited nature of the observational data available, we wish to apply simple models with a minimum of parameters. For this purpose we employ the similarity solutions for disk evolution discussed by Lynden-Bell & Pringle (1974), which assume that the viscosity has a power-law radial dependence and is independent of time. These similarity solutions provide an analytic form that is especially helpful in understanding the interplay of parameters. Although the problem can be solved numerically for any initial distribution of Σ, the use of a similarity solution avoids the introduction of additional parameters that are difficult to constrain. Moreover, Lynden-Bell & Pringle (1974) showed that disk structure will asymptotically approach the similarity solution at large times, regardless of specific initial conditions. (Lin & Bodenheimer 1982 showed that similarity solutions for disk evolution can result even in more complex situations, but given the limited nature of the available observations we restrict our discussion to the simplest case.)

The overall properties of these solutions can be understood in a simple way, starting from the viscous timescale,

$$t_{\rm visc} \sim R^2/\nu , \quad (11)$$

where ν is now the viscosity.[4] If the viscosity is a power law $\nu \propto R^\gamma$, then

$$\frac{dR_{cd}}{dt} \propto \frac{R_{cd}}{t_{\rm visc}} \propto R_{cd}^{(\gamma-1)} , \quad (12)$$

so that the variation of disk size with time is given by

$$R_{cd} \propto t^{1/(2-\gamma)} . \quad (13)$$

From conservation of angular momentum it follows that

$$M_d \propto t^{-1/[2(2-\gamma)]} , \quad (14)$$

and the variation of mass accretion rate can be found by differentiating equation (14) with respect to time.

Although it is unlikely that real disk viscosities are power-law functions of radius or are independent of time, the similarity solutions provide reasonable starting points. In addition, qualitatively new features not present in current treatments of T Tauri disk structure are introduced by simply allowing the disk to expand (Lin & Bodenheimer 1982; see also Stepinski 1997).

4.1. *General Equations*

The evolution of the surface density Σ of a thin Keplerian disk subject to the gravity of a point mass M is given by (Pringle 1981)

$$\frac{\partial \Sigma}{\partial t} = \frac{3}{R}\frac{\partial}{\partial R}\left[R^{1/2}\frac{\partial}{\partial R}(R^{1/2}\nu\Sigma)\right], \quad (15)$$

where ν is the viscosity. If the ν can be written as a power law in R independent of time,

$$\nu \propto R^\gamma , \quad (16)$$

then equation (15) has a similarity solution (Lynden-Bell & Pringle 1974), given by

$$\Sigma = \frac{C}{3\pi\nu_1 r^\gamma} T^{-(5/2-\gamma)/(2-\gamma)} \exp\left[-\frac{r^{(2-\gamma)}}{T}\right], \quad (17)$$

in which we have introduced the definitions

$$r \equiv R/R_1 , \quad \nu_1 \equiv \nu(R_1) , \quad (18)$$

where R_1 is a radial scale factor and C is a scaling constant. The nondimensional time T is

$$T = t/t_s + 1 , \quad (19)$$

where the viscous scaling time is

$$t_s = \frac{1}{3(2-\gamma)^2}\frac{R_1^2}{\nu_1} . \quad (20)$$

Thus, the scaling time is basically the viscous timescale of the disk at cylindrical radius R_1 (cf. Pringle 1981). For $t \ll t_s$, $T \sim 1$ and little evolution occurs.

Given this solution for Σ, expressions can be written for the mass flow, the radial velocity, and the torque or the angular momentum. The mass flux can be written as

$$\dot{M}(R,t) = CT^{-(5/2-\gamma)/(2-\gamma)} \exp\left(-\frac{r^{(2-\gamma)}}{T}\right) \times \left[1 - \frac{2(2-\gamma)r^{(2-\gamma)}}{T}\right]. \quad (21)$$

In the limit that r goes to zero,

$$\dot{M}/\Sigma = 3\pi\nu_1 r^\gamma = 3\pi\nu(r) , \quad (22)$$

which is the steady disk result. Because of the expansion necessary to conserve angular momentum, the mass flux in the evolving disk changes sign at a radius R_t, where

$$R_t = R_1\left[\frac{T}{2(2-\gamma)}\right]^{1/(2-\gamma)} . \quad (23)$$

The net motion of disk material at $R > R_t$ is outward, while for $R < R_t$ matter is accreting. This transition radius moves outward as the disk evolves.

[4] In this and following sections we generally use ν for viscosity, while subscript ν denotes frequency; the meaning should be clear from the context.

The mass distribution of the disk is given by

$$M_d(R, t) = M_d(t)\{1 - \exp\,[(R/R_1)^{2-\gamma}/T]\} \quad (24)$$

$$= M_d(t)\left\{1 - \exp\left[\frac{(R/R_t)^{(2-\gamma)}}{2(2-\gamma)}\right]\right\}, \quad (25)$$

where

$$M_d(t) = M_d(0)T^{-1/[2(2-\gamma)]} \quad (26)$$

is the total disk mass at time t.

We note two general results for the case $T \gg 1$, corresponding to times much longer than the viscous time; when the disk has evolved substantially and precise initial conditions are not important. In this limit the accretion rate onto the central star ($r \to 0$) approaches

$$\dot{M}(t) \propto t^{-(5/2-\gamma)/(2-\gamma)} \propto t^{-\eta}\,, \quad (\gamma < 2) \quad (27)$$

independent of the initial conditions, disk mass, radius, etc. The decay rate does not depend upon the absolute value of the viscosity, but instead on the radial dependence of the viscosity,

$$\gamma = \frac{(2\eta - 5/2)}{(\eta - 1)} \quad (\eta > 1)\,. \quad (28)$$

Thus, in principle, the observed value of η can be used to infer γ, although current limits yield great uncertainty (§ 4.3).

We also consider how the disk size scales with time in the limit $T \gg 1$. We use the transition radius R_t as a scaling point to illustrate the expected properties. If we evaluate the viscosity ν at a fixed arbitrary radius R_0, we have

$$R_t = R_1\left(\frac{3t\nu_0 R_1^{-(2-\gamma)}}{2R_0^{\gamma}}\right)^{1/(2-\gamma)}\,. \quad (29)$$

At long times, the disk has expanded so much that its initial radius does not affect its size, which is controlled instead by the magnitude of the viscosity and the age. Note that by using equation (23), and identifying R_t as an appropriate characteristic scaling radius $\propto R_{cd}$ for the similarity solution, one can use the equation of angular momentum conservation (eq. [10]) to derive equations (26) and (27).

4.2. *Viscosity*

The main difficulty in solving equation (15) is the lack of an appropriate prescription for the viscosity. Current studies suggest that the so-called "Balbus-Hawley" magnetorotational instability (Balbus & Hawley 1991; Hawley & Balbus 1991; Stone et al. 1996; Brandenburg et al. 1996) is the most likely candidate for producing the necessary viscous dissipation and angular momentum transport in disks. While these theoretical developments are promising, quantitative predictions of viscosities are uncertain.

Viscosities are often described using the α parameterization, which we use in the form (Pringle 1981)

$$\nu = \alpha c_s H\,, \quad (30)$$

where c_s is the sound speed in the disk and H is the scale height, and the α parameter is assumed to be less than unity. We can translate the magnitude of the required viscosity into the α formalism from the following considerations. If the disk is vertically (not radially) isothermal, then $H = c_s/\Omega(R)$.

Substituting, we find

$$\nu \propto \alpha T_d R^{3/2}\,, \quad (31)$$

where T_d is the disk temperature at R. If α is constant, and if $T_d \propto R^{-q}$, then the viscosity has a radial power-law dependence with exponent

$$\gamma = 3/2 - q \quad (\alpha = \text{constant})\,. \quad (32)$$

If $q = \frac{1}{2}$, then $\gamma = 1$.

The temperature structure of real disks is unlikely to follow a strict power law. Even in a steady, optically thick accretion disk, where the surface temperature is $T_{\rm eff} \propto R^{-3/4}$, the central temperature $T_c^4 \propto \tau T_{\rm eff}^4$, can vary in a non–power-law fashion because of changes in opacity that affect the disk optical depth τ. However, irradiation from the central star dominates the disk heating for most T Tauri stars (Kenyon & Hartmann 1995); at large disk radii, the external heating and the modest optical depths imply that the disk is fairly isothermal in the vertical direction, and the flaring of the outer disk causes $q \to \frac{1}{2}$ (Kenyon & Hartmann 1987). The observed variation of disk spectral index with wavelength of observation supports this variation of temperature gradient with radius (Kenyon & Hartmann 1995), and the detailed vertical structure calculations of D'Alessio et al. (1998) are consistent with these observations. Since most of the disk mass lies at large radii, we make the approximation $q \sim \frac{1}{2}$, which is also reasonably consistent with estimates for the outer disk temperatures of T Tauri stars (BSCG). With this approximation, consistent with the main disk heating mechanism being irradiation, the α = constant hypothesis implies $\gamma \sim 1$, nearly independent of time. However, if the evolutionary calculations are followed for a long enough period of time, the decrease in the stellar luminosity as the central T Tauri star contracts down its Hayashi track should be taken into account.

4.3. *Comparison with Observations*

The similarity solutions for disk evolution have four parameters: the initial disk mass, the initial disk characteristic radius (which is not important at large ages), the value of the viscosity at a specified radial distance, and the radial dependence of the viscosity γ. There are a similar number of observational constraints available at present (although several are not accurately known). The mass accretion rate measurements may be characterized in terms of three independent quantities; a mean or median accretion rate at a reference time ($t \sim 10^6$ yr), the decay rate η, and an estimate of the spread in accretion rates at a given age. Dust emission masses (or its essential equivalent, millimeter-wave emission) represent an additional observational quantity. Finally, estimates of disk sizes (e.g., Dutrey et al. 1995) provide yet another observational constraint for a few objects. Given the limited and approximate nature of the observational results, it is evident that the four-parameter similarity solutions provide a reasonable basis for an initial exploration of disk evolution and that the application of more complicated models with additional parameters is not justified at present.

As noted in § 4.1, a measurement of the decay rate η in the mass accretion rate can provide an estimate of γ. However, it is clear by considering the large uncertainties in η in the context of equation (28) that current observations do not meaningfully constrain γ. We therefore limit our discussion to two illustrative cases.

4.3.1. *Results for* $\gamma = 1$

For this case, the surface density is

$$\Sigma = \frac{M_d(0)}{2\pi R_1^2} \frac{1}{(R/R_1)T^{3/2}} e^{-(R/R_1)/T} , \quad (33)$$

the disk mass interior to R is

$$M_d(R, t) = M_d(0)T^{-1/2}\left\{1 - \exp\left[-\frac{R}{(R_1 T)}\right]\right\} , \quad (34)$$

and the mass accretion rate is

$$\dot{M} = \frac{M_d(0)}{2t_s} \frac{1}{T^{3/2}} e^{-(R/R_1)/T}\left[1 - \frac{2(R/R_1)}{T}\right] \quad (35)$$

with

$$t_s = \frac{1}{3} \frac{R_1^2}{\nu_1} . \quad (36)$$

The constant in equations (17) and (21) has been evaluated in terms of the initial disk mass $M_d(0)$. According to equations (24) and (25), R_1 is the radius where ~ 0.6 of the mass resides initially; at any time, ~ 0.4 of the mass is inside R_t.

Most T Tauri stars in Taurus have luminosities $\sim 1\ L_\odot$, and irradiation heating leads to a typical disk temperature $T_d \sim 10$ K at 100 AU (D'Alessio et al. 1998). (This is also consistent with observational estimates from spectral energy distributions of typical T Tauri stars, as indicated by the results of BSCG.) The typical mass of the stars is $M_* \sim 0.5\ M_\odot$ (see Table 1). Using these results, and the viscosity prescription equation (31), we can write the above solutions in terms of typical values for the expected disk quantities:

$$t_s \sim 8 \times 10^4 \left(\frac{\alpha}{10^{-2}}\right)^{-1} \left(\frac{R_1}{10\ \mathrm{AU}}\right) \left(\frac{M_*}{0.5\ M_\odot}\right)^{1/2} \left(\frac{T_{d2}}{10\ \mathrm{K}}\right)^{-1} \mathrm{yr} , \quad (37)$$

$$\Sigma \sim 1.4 \times 10^3 \frac{e^{-r/T}}{rT^{3/2}} \left(\frac{M_d(0)}{0.1\ M_\odot}\right) \left(\frac{R_1}{10\ \mathrm{AU}}\right)^{-2} \mathrm{g\ cm^{-2}} , \quad (38)$$

$$\dot{M} \sim 6 \times 10^{-7} \frac{e^{-r/T}}{T^{3/2}} \left(1 - \frac{2r}{T}\right) \left(\frac{R_1}{10\ \mathrm{AU}}\right)^{-1} \times \left(\frac{M_*}{0.5\ M_\odot}\right)^{-1/2} \left(\frac{T_{d2}}{10\ \mathrm{K}}\right) M_\odot\ \mathrm{yr}^{-1} , \quad (39)$$

where T_{d2} is the disk temperature at 100 AU. Finally, the expansion of the disk can be described by

$$R_t = 5T\left(\frac{R_1}{10\ \mathrm{AU}}\right)\mathrm{AU} . \quad (40)$$

This case ($\gamma = 1$) is the same as that considered by Hayashi (1981) in calculations of the evolution of the solar nebula. Hayashi estimated that the surface density varies as $\Sigma \propto R^{-3/2}$ without solving the equations directly. The similarity solution shows that this is not quite correct, as can be seen immediately from the requirement that the disk approach a steady state $\Sigma \propto \nu^{-1} \propto R^{-1}$ at radii much smaller than R_t.

The disk mass is determined by the initial disk mass $M_d(0)$ and the time parameter T, i.e., the number of viscous timescales that have elapsed. The viscous time t_s sets the timescale for initial disk evolution;

$$t_s \propto R_1 M_*^{1/2} (\alpha T_{d2})^{-1} . \quad (41)$$

For stars of similar mass and luminosity such as in the present sample, we expect that T_{d2} and M_* do not vary much. Keeping these parameters constant, the disk mass is set by the initial condition for ages $t \ll t_s$, while at large times the disk mass $M_d(t) \propto M_d(0)(R_1/\alpha)^{1/2}$. Thus, we expect that disks with the same initial mass and the same ratio of R_1/α will have the same $M_d(t)$ and $\dot{M}(t)$. However, these disks would have different sizes at a given time t,

$$R_t = \frac{R_1}{2} + 5\left(\frac{\alpha}{10^{-2}}\right)\left(\frac{M_*}{0.5\ M_\odot}\right)^{-1/2}\left(\frac{T_{d2}}{10\ \mathrm{K}}\right) \times \left(\frac{t}{8 \times 10^4\ \mathrm{yr}}\right)\mathrm{AU} . \quad (42)$$

For $T \gg 1$ the disk size grows linearly with time. On timescales $t \ll t_s$, the disk does not evolve greatly; thus, increasing t_s slows the rate of disk evolution accordingly.

Figure 3 shows results for a few different initial conditions. In all cases the models assume $M_* = 0.5\ M_\odot$ and $T_{d2} = 10$ K. The heavy solid line shows the "fiducial" model for the parameters $M_d(0) = 0.1\ M_\odot$, $\alpha = 10^{-2}$, and $R_1 = 10$ AU. The lighter solid line is for a model with the same parameters but with an initial disk mass $M_d(0) = 0.01\ M_\odot$, while the dotted line is again the same but with $M_d(0) = 0.2\ M_\odot$. The mass accretion rates shown in the upper left panel decrease in exact proportion to the initial mass, as do the disk masses shown in the lower left panel.

In the upper right panel we plot the half-mass disk radius (cf. eq. [34])

$$R(1/2) = 2(\ln 2)^{1/2} R_t . \quad (43)$$

The heavy solid, light solid, and dotted lines overlap in this figure because these disk models all have the same initial radii and viscous timescales. Comparison of $R(1/2)(t)$ with $\dot{M}$ and M_d shows how the expansion of the disk is related to the accretion rate and the remaining disk mass (cf. eq. [10]). At early times, the evolution is slower because T is not very large; only when the elapsed time is long in comparison with the initial characteristic viscous time of the disk t_s do the asymptotic forms of disk evolution take hold.

We also considered models with differing t_s, which would result from changing either the initial radius or α. For example, infall models for Taurus protostars suggest that the initial disk radii might be closer to 100 AU (Kenyon, Calvet, & Hartmann 1993). The short-dashed and the dot-dashed curves correspond to models with the standard fiducial parameters except that $R_1 = 50$ and 100 AU, respectively. Because these larger initial disk radii increase the viscous scaling time t_s, the mass accretion rate is lower for a fixed initial disk mass, and the decay of disk masses and accretion rates is slower; this causes the slope of the $\dot{M}(t)$ versus t to flatten out somewhat from the limiting case of $\eta = 1.5$ as $T \gg 1$. However, as shown in the upper right panel, the disk sizes eventually approach a similar value, expanding nearly linearly with time.

In the case of the model with $\alpha = 10^{-3}$, shown in long dashes in Figure 3, the scaling time is larger and the rate of growth of the disk is smaller (eq. [42]); as shown in the upper right panel of Figure 3, disk sizes do not grow significantly until after a few million years have elapsed.

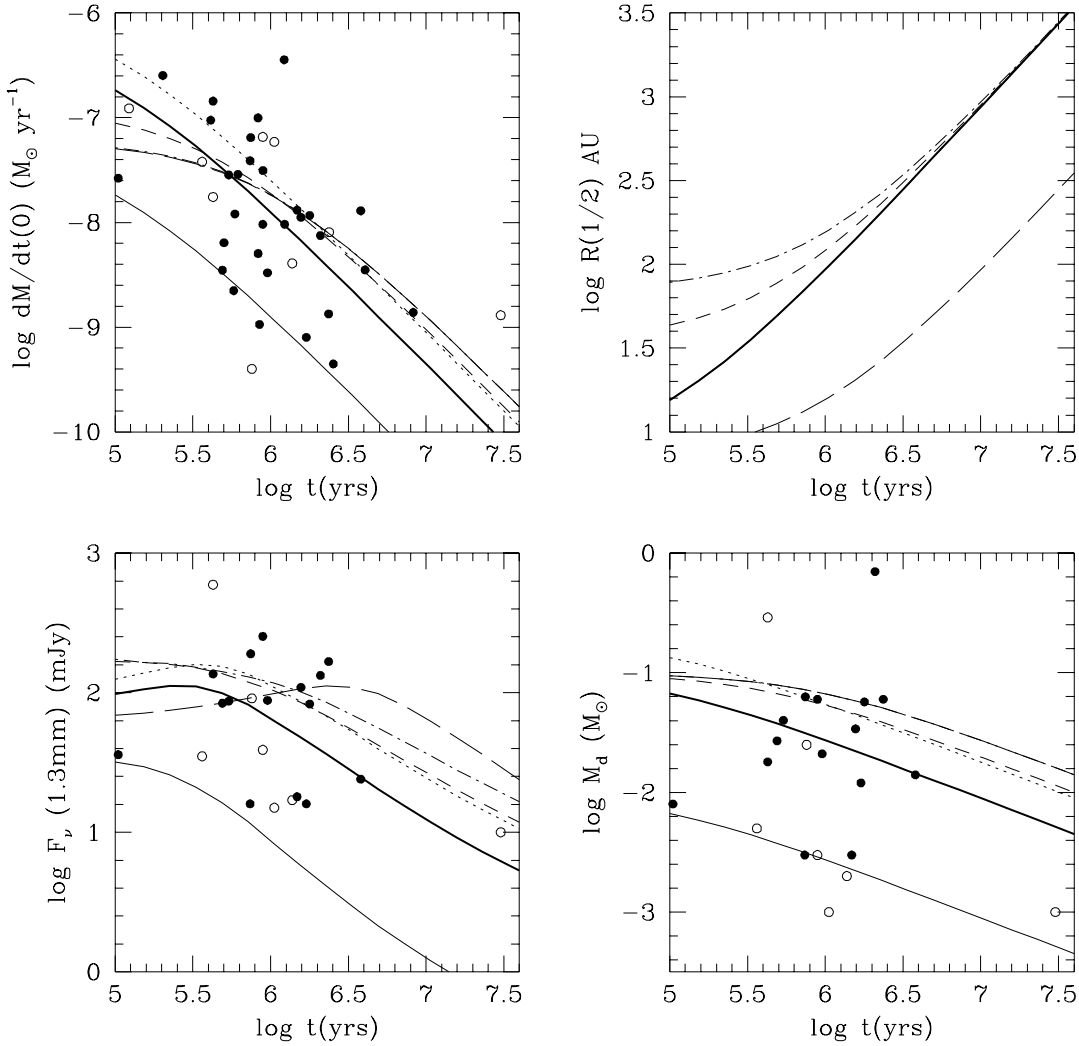

FIG. 3.—Properties of similarity solutions with $\gamma = 1$ (corresponding to $\eta = 1.5$) compared to Taurus observations. *Heavy solid line*, fiducial model, with parameters $M_d(0) = 0.1\ M_\odot$, $\alpha = 10^{-2}$, and $R_1 = 10$ AU. All other solutions have the same parameters as the fiducial model but one, as indicated in the following. *Long-dashed line*, $\alpha = 10^{-3}$. *Short-dashed line*, $R_1 = 50$ AU. *Dot-dashed line*, $R_1 = 100$ AU. *Dotted line*, $M_d(0) = 0.2\ M_\odot$. *Light solid line*, $M_d(0) = 0.01\ M_\odot$. In all cases the models assume $M_* = 0.5\ M_\odot$ and $T_d(100\ \text{AU}) = 10$ K. *Upper left*, mass accretion rate onto the star. Observations: Taurus sample, as in Fig. 1. *Upper right*, half-mass radius. *Lower left*, 1.3 mm fluxes. *Lower right*, Disk mass. *Filled circles*, single or unknown multiplicity stars; *open circles*, binaries. Observations: references in Table 3.

To facilitate comparison with observations, we also computed the disk emission at 1.3 and 2.7 mm assuming that the disk is vertically isothermal at $T(R)$, using the equation

$$F_\nu = \int_0^\infty dR\mu 2\pi R B_\nu\, T(R)[1 - \exp\,(-\tau_\nu/\mu)]/(4\pi d^2)\ , \quad (44)$$

where $\mu = 0.5$ is the cosine of the assumed average inclination angle, B_ν is the Planck function, the optical depth is

$$\tau_\nu = \kappa_\nu \Sigma(R)\ , \quad (45)$$

using a distance $d = 140$ pc. We adopted the dust opacity used by BSCG, $\kappa_\nu = 0.1(\nu/10^{12}\ \text{Hz})$ g cm^{-2}. Table 3 summarizes the data used for comparison and gives the appropriate references.

The similarity solution predicts that the disk temperature should fall to arbitrarily low temperatures at large times. In contrast, detailed calculations suggest that cosmic-ray heating might provide a minimum baseline temperature below which the disk cannot fall (D'Alessio et al. 1998). For the purposes of computing disk fluxes at 1.3 mm and spectral indices $\nu F_\nu \propto \nu^s$ between 1.3 and 2.7 mm, we did not allow disk temperatures to fall below 7 K. This assumption is formally inconsistent with our power-law similarity solution (unless α varies in a compensatory fashion), but since we have no data for stars with very large, cold disks, we ignore this complication in the present discussion.

The lower left panel in Figure 3 shows the 1.3 mm emission predicted for the various model parameters. The models predict relatively little variation with age, and mostly reflect differing disk masses. It is straightforward to show that, in the limit that the disk is entirely optically thin at frequency ν, the observed flux should vary as

$$F_\nu \propto M_d T_0 M_*^{1/2} (\alpha t)^{-1/2}\ . \quad (46)$$

The dependence on time and mass in the actual models is weaker than this because of optical depth effects. This is made clearer in Figure 4, where we show the spectral index

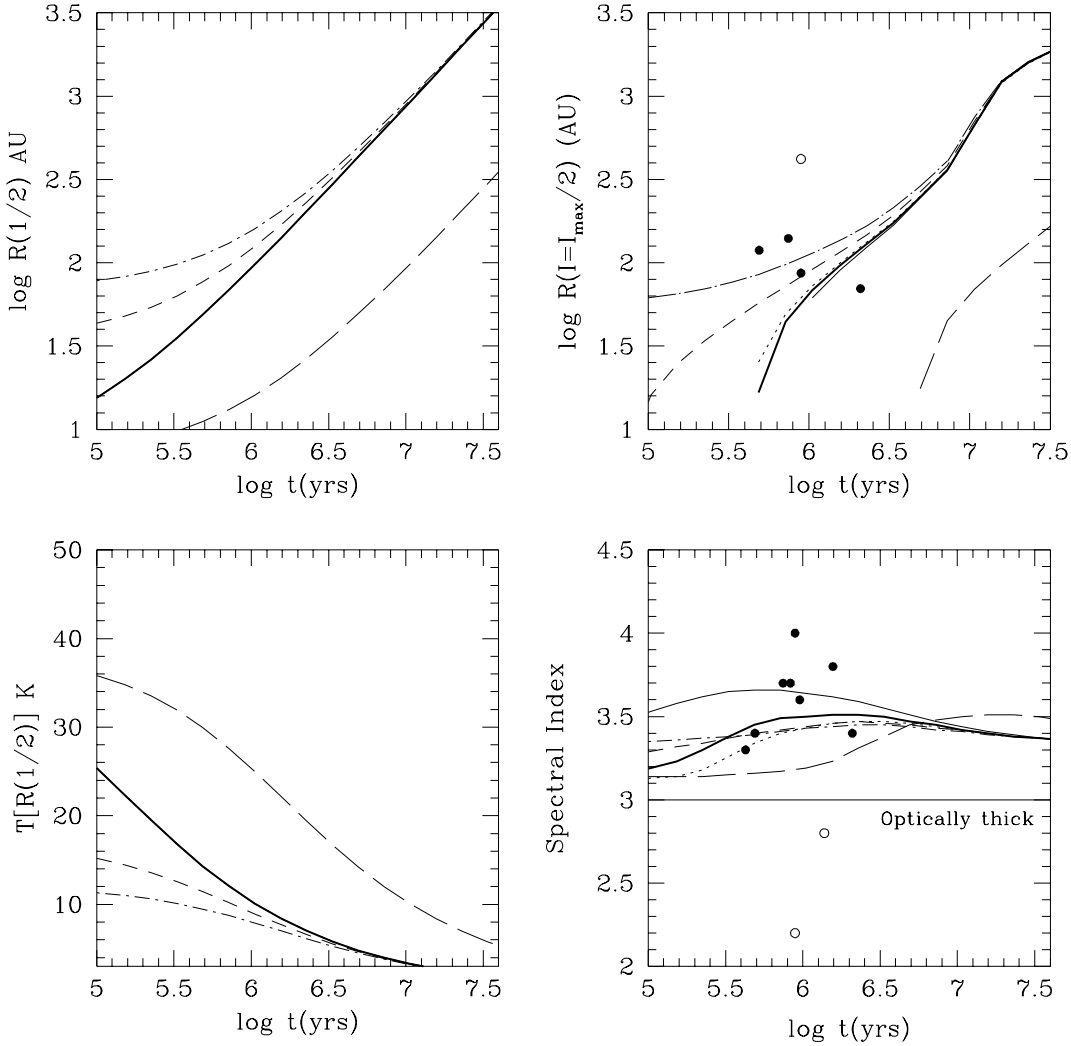

FIG. 4.—Additional properties of the models shown in Fig. 3. The half-mass radius is repeated (*upper left*) for ease of comparison. *Lower left*, temperature at half-mass radius. *Lower right*, spectral index, defined as log [νF_ν(1.3 mm)/νF_ν(2.7 mm)]/log [ν(1.3 mm)/ν(2.7 mm)]; the optically thick limit is marked. *Upper right*, estimated sizes at 2.7 mm from Dutrey et al. (1995), compared with model predictions calculated as described in the text. Symbol meanings are the same as in Fig. 3.

between 1.3 and 2.7 mm in the lower right panel. If the disk were optically thin, $s = 3 + \beta = 4$ (where β is the opacity dependence in frequency); lower values indicate the importance of emission from optically thick regions. At long times, the disk expands so much that the importance of optically thick emission decreases. In this limit one would predict $F_\nu \propto t^{-1}$, but the calculated fluxes fall off more slowly than this because of the limiting outer temperature adopted. The left lower panel of Figure 4 shows the temperature at the half-mass radius, which provides an indication as to the importance of the cutoff temperature in controlling the predicted fluxes and spectral indices.

In the upper right panel of Figure 4 we also show the apparent 2.7 mm sizes calculated for the similarity models, for comparison with the IRAM observations of Dutrey et al. (1995). The two-dimensional brightness distribution of the disk model has been convolved with a Gaussian that approximates the beam size used in the observations ($\sim 3'' \times 3''$). The convolved brightness distribution was fitted with a Gaussian, whose size (FWHP) is calculated along each axis. To compare with sizes reported by Dutrey et al. (1995), the deconvolved "Gaussian" size is calculated assuming the source has a Gaussian brightness distribution; in this case, the square of the convolved size is the sum of the squares of the deconvolved size and the beam size.

The apparent sizes generally scale with the half-mass radius (Fig. 4, *upper left*), although optical depth effects cause differences at early and late times. For $\alpha = 10^{-2}$ and ages between $\sim 3 \times 10^5$ and $\sim 3 \times 10^6$ yr, the size is of the order of 1″ ($\sim$140 AU at 140 pc). In this interval the disk has an inner, optically thick and bright region, which has a large contrast with the outer fainter regions, so the FWHP size does not change appreciably. Once most of the disk becomes optically thin, the contrast between inner and outer regions decreases and the size increases since most of the emission comes from the expanding large radii where most of the disk mass resides. This can also be seen comparing the sizes of models with initial mass 0.1 and 0.01 $M_\odot$. The latter has larger sizes because it is more optically thin everywhere. On the other hand, the model with $\alpha = 10^{-3}$ does not start to be resolved until $\sim 3 \times 10^6$ yr. In this case, since the characteristic timescale is larger, the disk does not

start evolving until much later. Also, the inner regions, where $\Sigma \propto \alpha^{-1}$, (eq. [22]), are more optically thick, so the contrast between the central and outer disk brightness stays larger for a longer time.

Comparison with the observations of Taurus stars in Figures 3 and 4 suggests that these similarity models are consistent with observations using reasonable parameters. For mass accretion rates, disk masses, and mm fluxes, the most important parameter is the disk mass—which, for the models shown, is mostly controlled by the initial disk mass. The models suggest that most of the observed variation in $\dot{M}$ can be accounted for by varying initial disk masses between 0.01 and 0.2 $M_\odot$, corresponding to disk masses at $t \sim 1$ Myr between ~ 0.003 and ~ 0.1 $M_\odot$. This conclusion is reinforced in the bottom right panel of Figure 3, where we compare with dust-emission disk masses from BSCG and OB (cf. § 3). Because BSCG and OB estimate disk masses by assuming power-law surface density and temperature structure, one might be concerned that there would be systematic differences using the disk structure of the similarity solution. However, the calculated mm fluxes (Fig. 3, *bottom left*) and spectral indices (Fig. 4, *bottom right*) compare quite well with the observations, indicating that there is no significant systematic effect introduced by the similarity disk structure on mass estimates from mm fluxes.

From the preceding discussion it is apparent that α cannot be determined without an estimate of disk size. The mm sizes observed by Dutrey et al. (1995), coupled to the mass accretion rates and disk masses, place very strong constraints on the value of α. Included in Table 3 are the sizes for the few stars reported by Dutrey et al. (1995), and these are plotted in the upper right hand panel of Figure 4. These stars have ages between 5×10^5 and 10^6 yr, and sizes $\sim 1''$–$2''$ (except for UY Aur). Models with $\alpha = 10^{-2}$ predict sizes entirely consistent with these observations. On the other hand, if α was much smaller, disks around ~ 1 Myr stars, which produce values of mass accretion rates and disk masses comparable to the observations, should not be resolvable. A model with $\alpha = 10^{-3}$ could produce sizes of order $1''$ if R_1 was increased to ~ 100 AU; this would require no disk evolution. However, in this case the mass accretion rate would be essentially constant, and low, over the range of ages covered by the T Tauri stars (see eqs. [37] and [39]), in disagreement with observed values. At the other extreme, if α is larger than $\alpha = 10^{-2}$, the characteristic time for evolution would be much shorter; in addition to having sizes larger than observed at 1 Myr, the disks would have significantly depleted their mass, so neither the mm fluxes, nor the masses, nor the mass accretion rates would agree with observations. We conclude that for typical disk radii of order 100 AU at 1 Myr (and $\gamma = 1$), $\alpha \sim 10^{-2}$ and initial disk masses in the range of $0.01 - 0.2$ $M_\odot$ satisfy the current observational constraints.

The model calculations assume that the disk's self-gravity is unimportant. To check, we calculate the Toomre Q parameter,

$$Q = \frac{c_s \kappa}{\pi G \Sigma} . \tag{47}$$

Setting the epicyclic frequency κ to equal the orbital frequency in the Keplerian disk, it is straightforward to show that the minimum value of Q, where the disk is most gravitationally unstable, occurs at $R(Q_{\min}) = 0.75 R_1 T$; using a mean molecular weight of 2, we find

$$Q_{\min} = 1.43 \left(\frac{M_d(0)}{0.1\ M_\odot}\right)^{-1} \left(\frac{M_*}{0.5\ M_\odot}\right)^{1/2} \times \left(\frac{T_{d2}}{10\ \mathrm{K}}\right)^{1/2} \left(\frac{R_1}{10\ \mathrm{AU}}\right)^{1/4} T^{3/4} . \tag{48}$$

At the earliest time shown in Figures 3 and 4, $t = 1 \times 10^5$ yr, $T = 2.25$ and $Q_{\min} = 2.63$ in our fiducial $M_d(0) = 0.1$ $M_\odot$ model. The $M_d(0) = 0.2$ $M_\odot$ model at this time has $Q_{\min} = 1.31$, so this model is initially near the limit for gravitational stability. For lower masses and at larger ages the models are more stable (e.g., Larson 1984; Lin & Pringle 1990; Shu et al. 1990).

An important caveat in this analysis is that binary (or multiple) systems cannot be treated. The gravitational torques due to a companion star can disrupt the disk, completely altering the evolution described by the similarity model. In Figures 3 and 4 we indicate known binary systems by open circles. While there is no evident effect of multiplicity on the mass accretion rates, there is a tendency for binaries to represent the lowest mm fluxes and corresponding masses, as noted previously (Jensen, Mathieu, & Fuller 1994, 1996; OB). Similarly, the few binary objects seem to have anomalous disk spectral indices and sizes (Fig. 4).

4.3.2. *Results for* $\gamma > 1$

As discussed in § 4.2, there is no theoretical basis at present for a constant α viscosity; and as pointed out in § 4.1, the constraints on γ are poor. Here we consider the general properties of models with larger values of γ. Since α is no longer constant, the value of the viscosity must be set at a fiducial radius. We have chosen to scale the viscosity to the value at 100 AU, defining it in term of the value of α at that radius, retaining the approximation $q = \frac{1}{2}$.

Solutions for a variety of parameters are shown in Figure 5. In general these models do not seem to be able to reproduce the range of observational constraints as well as the $\gamma = 1$ solutions. The reasons for this are easy to understand in the context of these analytic similarity solutions. For example, take the case $\eta = 2.5$, which corresponds to $\gamma = 5/3$. In this limit the disk expands in a rapidly accelerating manner, $R_t \propto T^{1/(2-\gamma)} \propto T^3$ (eq. [23]); correspondingly, $M_d(T) \propto T^{-1/[2(2-\gamma)]} \propto T^{-3/2}$ and $\dot{M}(T) \propto T^{-5/2}$ (eqs. [10], [26], and [27]).

Consider first the limit $T \gg 1$. In this case, the rapid expansion of the disk (Fig. 5, *upper right*) makes it difficult to satisfy reasonable constraints on disk sizes on early and late times. For reasonable disk sizes at $t = 1$ Myr, the initial disk size (half-mass radius) is very small, much smaller than typical estimates of disk sizes for very young stars (see above). Conversely, if one starts out with an initial disk half-mass radius of a few tens of AU at an age of ~ 0.3 Myr or less, then the disk sizes tend to become huge at ages $\gtrsim 1$–3 Myr. Such large disk radii are difficult to reconcile with current observational limits on disk sizes, and the large expansion factors imply such a rapid decrease in the disk mass that it is very difficult to explain the observed mm emission unless the initial disk masses are very large. To obtain some of the largest disk masses, ~ 0.1 $M_\odot$, at $t \sim 1$ Myr, with $T \gtrsim 4$ to obtain a steep decline in accretion rates, and $\eta = 2.5$, requires initial disk masses of $M_d \gtrsim 0.8$ $M_\odot$;

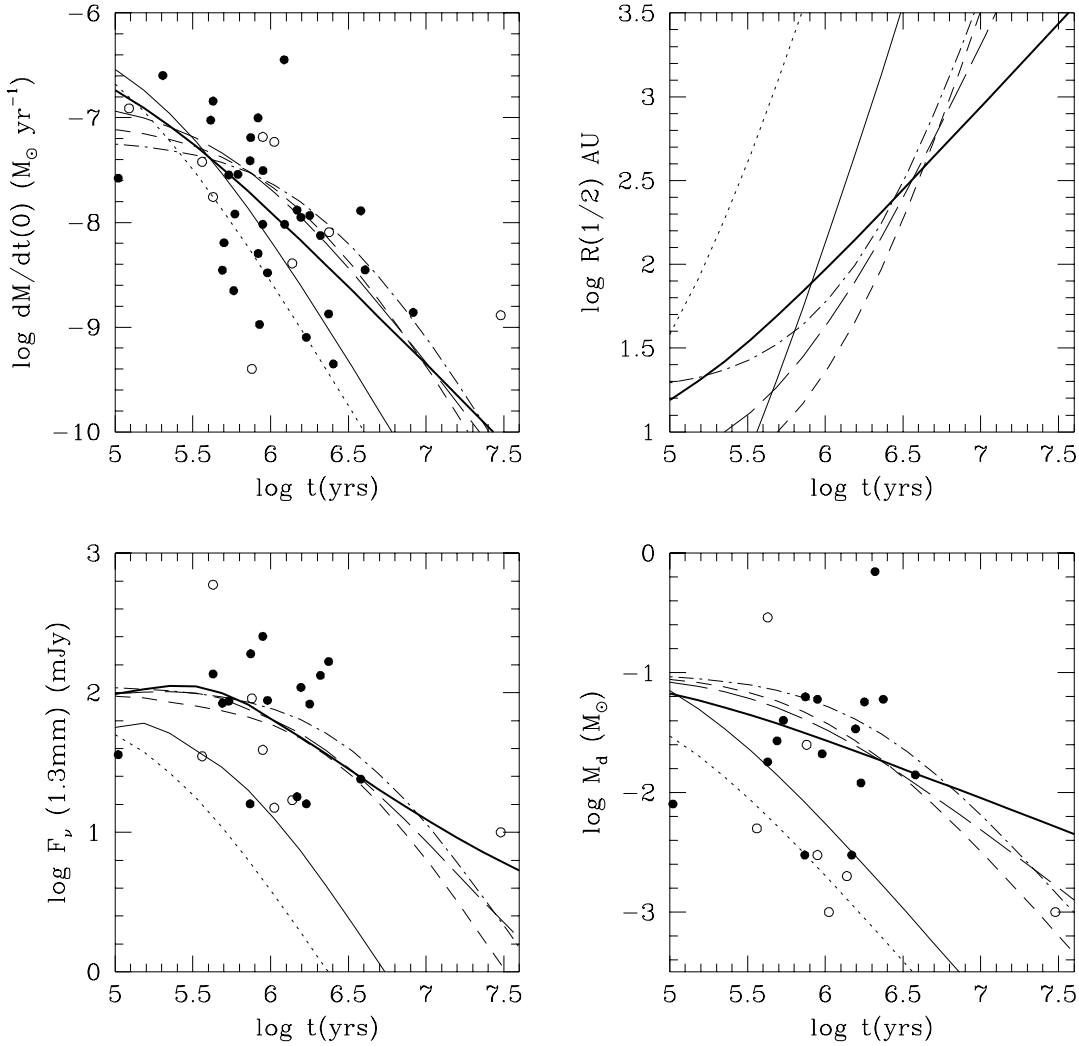

FIG. 5.—Properties of similarity solutions with differing values of γ. *Heavy solid line*, fiducial model, with properties as in Fig. 3, and $\gamma = 1$, $\eta = 1.5$. All other solutions have the same parameters as the fiducial model, except stated otherwise. *Long-dashed line*, $\gamma = 3/2$, $\eta = 2$. *Short-dashed line*, $\gamma = 5/3$, $\eta = 2.5$. *Dot-short-dashed line*, $\gamma = 5/3$, $R_1 = 50$ AU. *Dotted line*, $\gamma = 5/3$, $\alpha = 0.14$. *Light solid line*, $\gamma = 5/3$, $\alpha = 3 \times 10^{-2}$, $R_1 = 0.3$ AU, $M_d(0) = 0.2\ M_\odot$. Observational points as in Fig. 3.

such large disk masses are almost certainly gravitationally unstable (Larson 1984; Lin & Pringle 1990; Shu et al. 1990).

Alternatively, one might suppose that T is not a large parameter. In this limit, the evolution of the disk is slowed from its asymptotic value, so that disk sizes change within a smaller range, and disk masses and millimeter-fluxes are easier to explain. However, as shown in Figure 5, for cases where the viscous timescale is increased such that T is relatively small at $t = 1$ Myr, the corresponding effect is to slow the rate of decay of the mass accretion rate—which was the motivation to investigate large γ solutions in the first place.

In summary, it appears that the bulk of current observational constraints are more easily satisfied with $\gamma \sim 1$ than with $\gamma \gtrsim 3/2$. Studies of older pre–main-sequence stars are required to provide definite conclusions.

5. DISCUSSION

5.1. *Implications for Disk Structure*

Our new mass accretion rates tend to be lower than some previous estimates (though not all; Valenti, Basri, & Johns 1993), suggesting that viscous heating of the disk during the T Tauri phase is less important relative to irradiation heating by the central star than frequently assumed. The time decay of disk accretion, though uncertain, appears to be relatively rapid in comparison with some estimates of the timescales for planet formation (e.g., Podosek & Cassen 1994, and references therein).

The revised mass accretion rates, coupled with evolutionary timescales, indicate disk masses on average within a factor of 3 of the dust masses derived from millimeter-wave emission. This result suggests that there are no large systematic problems with long-wavelength dust opacities, at least in disks of ages $\lesssim 1$ Myr. While rapid evolution of grain properties is expected to occur over very short timescales, $\sim 10^3$ yr at 1 AU, (e.g., Weidenschilling & Cuzzi 1993), the agreement between the dust-emission masses and the inferred accretion masses suggests that changes in dust opacities on scales ~ 100 AU, where most of the disk mass resides, may be much slower. The results further suggest that most of the observed range of mass accretion rates in T Tauri stars can be explained with initial disk masses in the range 0.01–0.2 $M_\odot$, consistent with the notion that T Tauri accretion takes place after any rapid evolution due to gravi-

tational instability. They also imply that the change in central stellar mass during the bulk of the T Tauri phase ($\gtrsim 1$ Myr) is relatively small.

Constraints on viscosity currently are poorly determined from the decay of mass accretion rates. For $\gamma \sim 1$, consistent with our preferred fits to the decay of mass accretion rates, present measurements of disk sizes imply $\alpha \approx 10^{-2}$ on scales $\sim$10–100 AU. in agreement with some current simulations of the Balbus-Hawley instability (Stone et al. 1996; Brandenburg et al. 1996). For larger values of γ it is more difficult to estimate the appropriate magnitude of the viscosity; however, such models evolve so rapidly that it is difficult to reconcile them with observations (§ 4.3.2).

Figure 6 illustrates the surface density of the fiducial model ($\gamma = 1$) as a function of radius for three different times, 0.32, 1, and 3.2 Myr. At these times, the disk has $R_t = 25$, 70, and 212 AU, and mass 0.04, 0.03, and 0.015 $M_\odot$. The surface density of the fiducial model agrees reasonably well with that of the minimum mass solar nebula of Hayashi (1981) at early ages, but decreases substantially at ages $\gtrsim 1$ Myr; the total mass still remains comparable to that of the minimum mass nebula, but it now mostly resides at much larger radii than the solar system planets. The model surface density distribution must be considered to be schematic, especially at small radii. Temperature and viscosity distributions may well exhibit strong non–power-law behavior, due in part to enhanced opacity trapping of accretion-generated heat, which is especially important in the innermost disk regions (see, e.g., Cassen 1994, and references therein; D'Alessio et al. 1998). Our calculations, which focus on the expansion of the outer disk and the corresponding importance of irradiation in determining disk heating, are somewhat complementary to the recent evolutionary models of Stepinski (1997), who concentrated in more detail on the structure of the inner disk regions in which accretion heating dominates.

The surface density distributions of the similarity solutions differ from the usual assumptions used in disk modeling (cf. BSCG). For these solutions, much of the mass of the disk resides in the outer region $R > R_t$, where the surface density falls off (roughly) exponentially with increasing distance. The exponential behavior is a generic result for viscously expanding disks; the details of the solution will depend upon the precise value of γ, but the outer "edge" of the disk is not sharp. In this connection it is interesting to note that McCaughrean & O'Dell (1996) argued that the circumstellar disks seen in silhouette against the bright background of the Orion Nebula also have exponentially varying surface density distributions in their outer regions. Although the exponential edges of these disks may be created by a variety of effects (McCaughrean & O'Dell 1996), and photoevaporation and photodissociation may be dominant (Johnstone, Shu, & Hollenbach 1996), it is worth noting that the basic picture of viscous disk expansion also predicts exponential or quasi-exponential disk edges, assuming that the disks have expanded somewhat from their initial states. Furthermore, although the radii of the silhouette disks are also relatively large compared with Taurus estimates, ranging from about 25 AU to about 500 AU, they are not inconsistent with the standard models presented here for Taurus, even though the ages of the Orion Nebula stars may be $t \lesssim 10^6$ yr (Hillenbrand 1997). The essential point is that the dust opacity at visual wavelengths is quite large, so that shadow sizes represent the extreme tenuous outer disk regions. For a quantitative comparison, we can calculate the radius where the optical depth at a given wavelength is unity, R_λ. Assuming an opacity of 380 cm^2 g^{-1} at 0.5μ (Draine & Lee 1984), and using our $\gamma = 1$ solution, the implicit equation describing the evolution of $R_{0.5}$ with time is

$$\left(\frac{R_{0.5}}{R_1}\right) e^{(R_{0.5}/R_1)/T} = \frac{5.4 \times 10^5}{T^{3/2}} \left(\frac{M_d(0)}{0.1\ M_\odot}\right)\left(\frac{R_1}{10\ \mathrm{AU}}\right)^{-2} . \tag{49}$$

Inspection of this equation shows that $R_{0.5}$ will increase as long as $R_{0.5}/R_1 > T$ and will decrease as $T^{-3/2}$ for $R_{0.5}/R_1 \ll T$.

Figure 7 shows the radius where optical depth $\tau = 1$ at 0.5 μm, calculated for the same models in Figure 3. It is seen that the models with the fiducial Taurus parameters can easily explain disk sizes of order 500 AU at optical wave-

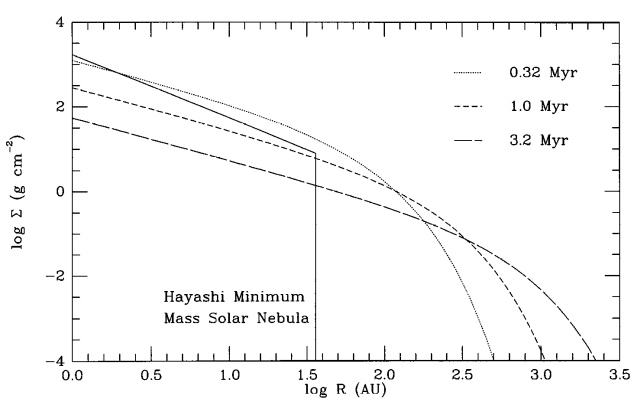

FIG. 6.—Surface density of the fiducial model, with parameters as in Fig. 3, for three different times: 0.32 Myr, 1 Myr, and 3.2 Myr. The Hayashi (1981) minimum mass solar nebula surface density distribution, $\Sigma \propto R^{-3/2}$, is plotted for reference.

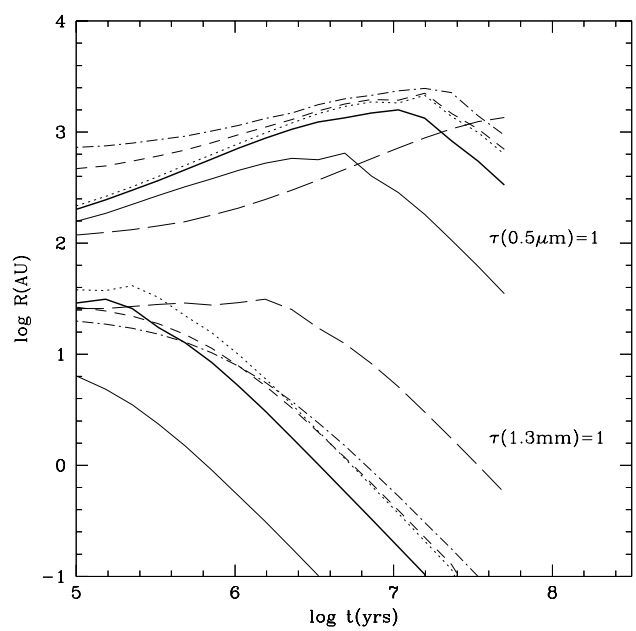

FIG. 7.—Radius where optical depth is equal to 1 at 0.5 μm (*upper set of lines*) and at 1.3 mm (*lower set of lines*). Models for $\gamma = 1$, labeled as in Fig. 3.

lengths. In contrast, the optically thick regions at millimeter wavelengths are much smaller, as also indicated in Figure 7. This difference reflects the fact that a very small amount of dust is required to produce significant absorption at optical wavelengths; the silhouettes are probing the outermost disk regions and are not good indicators of the total amount of material present. On the other hand, since most of the disk is optically thin at radio wavelengths, the emission depends directly on the total mass present. Comparisons between optical and millimeter-wave measurements of disk sizes can provide a test of the disk structure predicted here.

5.2. *Implications for Disk Evolution*

Although our results for disk accretion and consequent evolution are highly preliminary, they incorporate several independent astronomical constraints into a consistent physical picture with reasonable parameters. One of the messages of Figure 3 is that simple models predict relatively little evolution in many easily observable parameters, such as millimeter-wave disk fluxes; much of the range in long-wavelength fluxes and mass accretion rates may well derive from differing initial disk masses (which may in turn reflect effects of gravitating companions ignored here).

The models suggest that T Tauri disks may expand far beyond their initial sizes during their pre–main-sequence evolution. In this connection it is interesting to consider the β Pic stars, some of which have outer disk sizes of order 10^3 AU; the models in Figures 3 and 4 suggest that even low-mass stars might have such extended disks at ages of 10 Myr. (For $\gamma > 1$ disk expansion is even more rapid.) The ultimate fate of this material is uncertain, and other processes such as photoevaporation (Shu, Johnstone, & Hollenbach 1993) and tidal truncation need to be considered. Nevertheless, the expansion implied by the viscous disk solutions suggest that low-mass stars like the Sun might have had disk systems of appreciable mass that extended far beyond the limits of the present solar system planets at an age of 10 Myr or more (Tremaine 1990).

While the properties of inner disks may differ substantially from those of outer disks, the evolution of the outer disk may drive overall system behavior. For example, the similarity solutions formally extend the disk all the way to $R \to 0$, though there must be some inner boundary that affects disk properties. The inner boundary condition may be one of zero torque, as in the classical boundary layer solution at the stellar surface (Lynden-Bell & Pringle 1974), or in the case of an inner X-wind coupled to a stellar magnetosphere which carries away the accreted angular momentum at the corotation radius (Shu et al. 1994). Alternatively, it is possible that some angular momentum of the star is transferred back to the disk (Lynden-Bell & Pringle 1974; Ghosh & Lamb 1979; Shu et al. 1994; Cameron & Campbell 1993; Cameron, Campbell, & Quaintrell 1995; Armitage & Clarke 1996). In either case, the angular momentum inner boundary condition for the accretion disk does not strongly affect the overall evolution (Lynden-Bell & Pringle 1974; Lin & Bodenheimer 1982). The mass accretion rate is set by the expansion of the outer disk, while the surface density distribution at small radii is modified by the inner boundary condition.

It has been suggested that winds or jets may remove significant amounts of angular momentum from outer regions accretion disk (e.g., Königl 1989); this would eliminate the need for the outer disk to expand. However, we take the view that winds or jets are a phenomenon of only the innermost disk, for reasons outlined in Hartmann (1995; see also Pringle 1989 and Shu et al. 1994). In this case the wind/jet does not affect the overall problem greatly, since most of the mass to be accreted comes from outer disk regions where wind angular momentum loss is unimportant.

T Tauri accretion is now thought to proceed through a stellar magnetosphere rather than a boundary layer (Königl 1991; see also Bertout, Basri, & Bouvier 1988; Hartmann 1995). The decay of mass accretion rates with age suggest that, at some point, the stellar magnetosphere may be sufficiently strong so as to prevent accretion onto the central star (Lynden-Bell & Pringle 1974; Armitage & Clarke 1996). All other things being equal, for a dipolar stellar magnetic field one expects the magnetic truncation radius to vary as $R_m \propto \dot{M}^{-2/7}$ (Königl 1991); thus, in our standard solutions, the $t^{-3/2}$ decay of the accretion rate would suggest that the magnetospheric truncation radius would increase by a factor of about 2.5 as the star ages from 1 to 10 Myr. If the truncation radius is close to corotation at 1 Myr (Shu et al. 1994), then this scaling would imply a shut off of accretion, along with a corresponding elimination of the optical signatures—hot continuum and emission lines—of accretion.

It is highly unlikely that disks exhibit pure power-law viscosity over several orders of magnitude of radius. In general, differing viscosities in the inner disk will tend to modify the surface density distribution accordingly, while the mass accretion rate is set by the expansion of the outer disk (Cassen 1994; Stepinski 1997). This conclusion could be modified by time-dependent angular momentum transport. For example, in the model of Gammie (1996), only the layers of the disk within a column density ~ 100 g cm^{-2}, or hotter than about 1000 K, are "active"; regions not satisfying this constraint do not have sufficient ionization to effectively couple the magnetic field to disk material and allow the Balbus-Hawley instability to transfer angular momentum. In these low-ionization regions, mass builds up in the disk, probably leading eventually to an instability and a short phase of rapid accretion. We note that, in our standard model, the nonsteady region according to Gammie's prescription is confined to radii $\lesssim 3$ AU, so that the outer disk evolution is not strongly affected. Moreover, Gammie concluded that the low-state accretion rate is roughly $10^{-8}\ M_\odot$ yr^{-1}, comparable to the median values found here, suggesting that short-term variability using the Gammie prescription may occur within a modest range around the mean values predicted by our similarity models. Time-dependent calculations are needed to explore this question further.

6. CONCLUSIONS

We have shown a correlation between age and mass accretion rates for a sample of K5–M2 pre–main-sequence stars in Taurus. The precise form of this correlation is uncertain; for $\dot{M} \propto t^{-\eta}$, $\eta \sim 1.5$–2.8, with some preference for lower values of η considering likely errors and probable age corrections for birthline positions. The mass accretion rates, coupled with estimates of stellar ages, imply disk masses that are consistent with estimates from millimeter and submillimeter dust continuum emission, suggesting that the interpretation of the latter data is not subject to order-of-magnitude systematic errors from dust opacities.

Extrapolations of the present data suggest that accretion rates may fall so low that stellar magnetospheres can prevent accretion at ages $\gtrsim 10$ Myr. Viscosities are poorly constrained by the present data; however, similarity solutions with initial disk masses range from ~ 0.01 to $0.2\ M_{\odot}$, below the limit of gravitational instability, and viscosities parameterized by $\alpha \sim 10^{-2}$ are consistent with observations. The similarity solutions suggest that disks may possibly become quite large, ~ 1000 AU, by the end of pre–main-sequence evolution. Future observations of accretion rates in older pre–main-sequence stars can strongly constrain evolution of T Tauri disks.

This work was supported in part by NASA grants NAGW 2306 and NAG 5-4282. E. G. thanks the Swedish Natural Science Research Council for financial support.

REFERENCES

Armitage, P. J., & Clarke, C. J. 1996, MNRAS, 280, 458
Balbus, S. A., & Hawley, J. F. 1991, ApJ, 376, 214
Beckwith, S. V. W., & Sargent, A. I. 1991, ApJ, 381, 250
Beckwith, S. V. W., Sargent, A. I., Chini, R. S., & Güsten, R. 1990, AJ, 99, 924 (BSCG)
Bertout, C., Basri, G., & Bouvier, J. 1988, ApJ, 330, 350
Brandenburg, A., Nordlund, A., Stein, R. F., & Torkelsson, U. 1996, ApJ, 458, L45
Cameron, A. C., & Campbell, C. G. 1993, A&A, 274, 309
Cameron, A. C., Campbell, C. G., & Quaintrell, H. 1995, A&A, 298, 133
Cassen, P. 1994, Icarus, 112, 405
D'Alessio, P., Cantó, J., Calvet, N., & Lizano, S. 1998, ApJ, submitted
D'Antona, F., & Mazzitelli, I. 1994, ApJS, 90, 467
Draine, B. T., & Lee, H. M. 1984, ApJ, 285, 89
Dutrey, A., Guilloteau, S., Duvert, G., Prato, L., Simon, M., Schuster, K., & Menard, E. 1995, A&A, 309, 493
Gammie, C. F. 1996, ApJ, 457, 355
Gauvin, L. S., & Strom, K. M. 1992, ApJ, 385, 217
Ghosh, P., & Lamb, F. K. 1979, ApJ, 234, 296
Gullbring, E., Hartmann, L., Brice, C., & Calvet, N. 1997, ApJ, 492, 323 (Paper I)
Hartigan, P., Edwards, S., & Ghandour, L. 1995, ApJ, 452, 736
Hartmann, L. 1995, Rev. Mexicana Astron. Af., 1, 285
Hartmann, L., Cassen, P., & Kenyon, S. J. 1997, ApJ, 475, 770
Hawley, J. F., & Balbus, S. A. 1991, ApJ, 376, 223
Hayashi, C. 1981, Prog. Theor. Phys. Suppl., 70, 35
Hillenbrand, L. 1997, ApJ, AJ, 113, 1733
Jensen, E. L. N., Mathieu, R. D., & Fuller, G. A. 1994, ApJ, 429, L29
———. 1996, ApJ, 458, 312
Johnstone, D., Shu, F. H., & Hollenbach, D. 1996, J. R. Astron. Soc. Canada, 90, 319
Keene, J., & Masson, C. R. 1990, ApJ, 335, 635
Kenyon, S. J., Calvet, N., & Hartmann, L. 1993, ApJ, 414, 676
Kenyon, S. J., & Hartmann, L. 1987, ApJ, 323, 714
———. 1995, ApJS, 101, 117 (KH)
Königl, A. 1989, ApJ, 342, 208
———. 1991, ApJL, 370, L39
Larson, R. B. 1984, MNRAS, 206, 197
Lay, O. P., Carlstrom, J. E., Hills, R. E., & Phillips, T. G. 1994, ApJ, 434, L75
Lin, D. N. C., & Bodenheimer, P. 1982, ApJ, 262, 768
Lin, D. N. C., & Pringle, J. E. 1990, ApJ, 358, 515
Lüst, R. 1952, Z. Naturforsch, 7a, 87
Lynden-Bell, D., & Pringle, J. E. 1974, MNRAS, 168, 603
Mathieu, R. D. 1994, ARA&A, 32, 465
Mathis, J. 1990, ARA&A, 28, 37
Mazzitelli, I. 1989, in ESO Workshop on Low-Mass Star Formation and Pre–Main Sequence Objects, ed. B. Reipurth (Garching: ESO), 433
McCaughrean, M. J., & O'Dell, C. R. 1996, AJ, 111, 1977
Osterloh, M., & Beckwith, S. V. W. 1995, ApJ, 439, 288 (OB)
Podosek, F. A., & Cassen, P. 1994, Meteoritics, 29, 6
Pollack, J. B., Hollenbach, D., Beckwith, S., Simonelli, D. P., Roush, T., & Fong, W. 1994, ApJ, 421, 615
Press, W. H., Flannery, B. P., Teukolsky, S. A., & Vetterling, W. T. 1986, Numerical Recipes, the Art of Scientific Computing (Cambridge: Cambridge Univ. Press), 454
Pringle, J. E. 1981, ARA&A, 19, 137
———. 1989, MNRAS, 236, 37P
Ruden, S. P., & Pollack, J. B. 1991, ApJ, 375, 740
Ryu, D., & Goodman, J. 1992, ApJ, 338, 438
Schwartz, R. D. 1991, in Low-Mass Star Formation in Southern Molecular Clouds, ed. B. Reipurth (ESO Sci. Rep. 11), 93
Shakura, N. I., & Sunyaev, R. A. 1973, A&A, 24, 337
Shu, F., Johnstone, D., & Hollenbach, D. 1993, Icarus, 106, 92
Shu, F., Najita, J., Ostriker, E., Wilkin, F., Ruden, S., & Lizano, S. 1994, ApJ, 429, 781
Shu, F. H., Tremaine, S., Adams, F. C., & Ruden, S. P. 1990, ApJ, 358, 495
Simon, M., & Prato, L. 1995, ApJ, 450, 824
Simon, M., et al. 1995, ApJ, 443, 625
Skrutskie, M. F., Dutkevich, D., Strom, S. E., Edwards, S., Strom, K. M., & Shure, M. A. 1990, AJ, 99, 1187
Stahler, S. W. 1983, ApJ, 274, 822
———. 1988, ApJ, 332, 804
Steenman, H., & Thé, P. S. 1989, Ap&SS, 161, 99
Stepinski, T. 1997, Icarus, submitted
Stone, J. M., & Balbus, S. A. 1996, ApJ, 464, 364
Stone, J. M., Hawley, J. F., Gammie, C. F., & Balbus, S. A. 1996, ApJ, 463, 656
Strom, K. M., Strom, S. E., Edwards, S., Cabrit, S., & Skrutskie, M. F. 1989, AJ, 97, 1451
Tremaine, S. 1990, in Baryonic Dark Matter, ed. D. Lynden-Bell & G. Gilmore (Dordrecht: Kluwer), 37
Valenti, J. A., Basri, G., & Johns, C. M. 1993, AJ, 106, 2024
von Weizsäcker, C. F. 1948, Z. Naturforsch, 3a, 524
Weidenschilling, S. J., & Cuzzi, J. N. 1993, in Protostars and Planets III, ed. E. H. Levy & J. I. Lunine (Tucson: Univ. Arizona Press), 1031